

# R Aquarii spectra revisited by SUMA

Marcella Contini<sup>1\*</sup> and Liliana Formiggini<sup>2</sup>

<sup>1</sup>*School of Physics and Astronomy, Tel Aviv University, Tel Aviv 69978, Israel*

<sup>2</sup>*School of Physics and Astronomy, Tel Aviv University and the Wise Observatory, Tel Aviv 69978, Israel*

Accepted. Received ; in original form

## ABSTRACT

We analyse the optical spectra and the UV spectral evolution of the jets and of the HII region inside the R Aquarii binary system by the code SUMA which consistently accounts for shock and photoionization. The temperature of the hot star results 80,000 K as for a white dwarf. We find that the shock velocity in the NE jet increased between 1983 and 1989. The spectral evolution between 1989 and 1991 of the SW jet indicates that a larger contribution from low density-velocity matter affects the 1991 spectra. The evolution of the UV spectra from 8/11/1980 to 26/5/1991 in the HII region indicates that the reverse shock is actually a standing shock. The results obtained by modelling the line spectra are cross-checked by the fit of the continuum SED. It is found that a black-body temperature of 2800 K reproduces the radiation from the red giant. A black-body emission component corresponding to 1000 K is emitted by dust in the surrounding of the red giant. Model calculations confirm that the radio emission is of thermal origin. We found that the NE jet bulk emission is at a distance of about  $2 \cdot 10^{15}$  cm from the internal system, while the distance of the SW jet bulk is  $\sim 6 \cdot 10^{14}$  cm. The distance of the reverse shock from the hot source in the internal region is  $\leq 9 \cdot 10^{13}$  cm.

**Key words:** shock waves;stars: binaries: symbiotic-stars:individual: R Aqr

## 1 INTRODUCTION

The symbiotic star R Aquarii (R Aqr) is an interacting system of a long-period Mira variable (LPV) and a hot star. The optical light curve is dominated by the 386.83 day pulsation period of the LPV, while the presence of a hot companion and its accretion disk is inferred from the ultraviolet spectra. The binary system is characterized by a highly inclined orbit to the line of sight ( $i \sim 70$  degree) with large eccentricity ( $e \sim 0.8$ ), a semi-major axis of  $2.7 \cdot 10^{14}$  cm (Meier & Kafatos 1995), and an orbital period of  $\sim 44$  yr (Wilson et al 1981, Hinkle et al. 1989, Hollis, Pedelty, & Lyon 1997). A binary separation of 11 AU is evaluated adopting a distance to Earth  $d \sim 200$  pc (Solf & Ulrich 1985, Hollis et al. 1997; see also Viotti et. al 1997).

The binary system hosts a compact HII region within a filamentary oval nebula (Kafatos, Michalitsianos, & Hollis 1986) and is surrounded by a large and complex nebulosity. Two jets oriented at SW and NE have been detected and were observed at ultraviolet, optical, and radio wavelengths. The bipolar morphology of R Aqr detected by VLA data (Kafatos et al 1989) was confirmed by HST high resolution images (Paresce et al 1991, Paresce & Hack 1994). Meier &

Kafatos (1995, Fig. 1) show the position of the NE and SW jets with respect to the central region of R Aqr.

The extensive IUE monitoring of the spectra from the central HII region and from the NE and SW jets has been analysed by Hollis et al (1991) and Meir & Kafatos (1995). In particular, the HII region and the NE jet temporal changes show increasing emission line intensities from 1979 to 1989, while the SW jet shows a decrease by a factor of 1.5 between 1989 and 1991.

Both shocks and photoionization by the hot star have been evoked as the excitation mechanisms that produce the rich emission line spectra from the jets (Hollis et al 1991). The observed line ratios could not be explained by pure photoionization models and also shock dominated models (Binette et al 1985) were not successful to reproduce them. Some discrepancies also result from the modelling of Burgarella, Vogel, & Paresce (1992) who accounted for shock and photoionization by the hot source, which were not calculated in a consistent way.

In this paper we would like to investigate the R Aqr system adopting the colliding wind scenario. In symbiotic binaries the collision of the winds from the hot star and the red giant creates a complex hydrodynamic structure (Nussbaumer 2000 and references therein). The emitting gas

\* E-mail: contini@ccsg.tau.ac.il

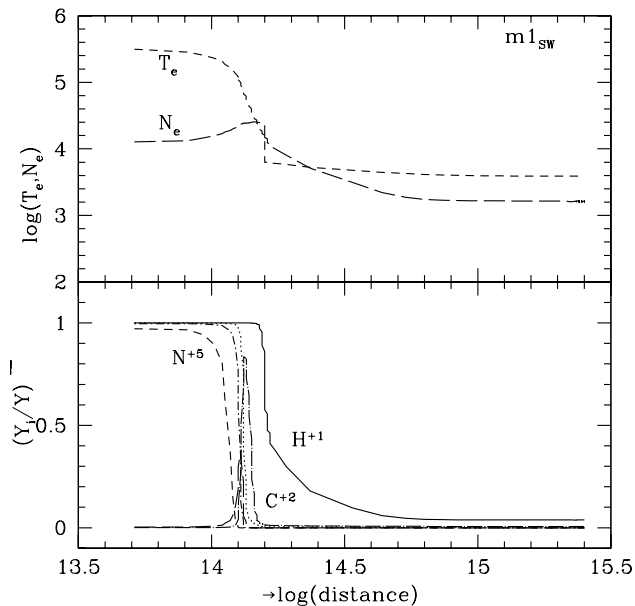


**Figure 1.** The shock front is on the left. bottom: The distribution of the fractional abundance throughout the nebula relative to model  $m1_{SW}$  of the ions  $N^{+5}$  (short-dashed line),  $C^{+4}$  (dot-dashed line),  $C^{+3}$  (long-dashed line),  $C^{+2}$  (long-dash-dot line),  $H^{+}$  (solid line),  $He^{+2}$  (dotted line); top: the distribution of the electron temperature and electron density.

within the system is then ionized and heated both by the photoionizing flux from the hot star and by shocks.

We will follow the same procedure as previously adopted for HM Sge (Formigini, Contini, & Leibowitz 1995), AG Peg (Contini 1997), RR Tel (Contini & Formigini 1999), etc., focusing on the physical conditions in the emitting nebulae by modelling the emission spectra in the central HII region and in the jets.

Models which consistently account for shock and photoionization from an external source are used (Sect. 2), adopting for the calculations the code SUMA (see Viegas & Contini 1994, Contini 1997, and references therein).

We will start by modelling the optical and UV line ratios in the SW and NE jets (Sect. 3). We will investigate the time evolution of the UV spectra from the HII region in Sect. 4, since no optical spectra are given for the internal region of R Aqr. The models will be cross checked by the agreement with the spectral energy distribution (SED) of the continuum (Sect. 5). Concluding remarks appear in Sect.

6

## 2 THE MODELS

Two shock fronts are created at collision of the winds between the stars, one propagating in reverse toward the hot star and the other propagating outwards the system. Recent observations of symbiotic novae show that spectra are also emitted from the downstream region of shocks propagating outside the system and eventually merging with the ISM (Contini & Formigini 2001).

The nebula between the stars is ionised and heated by

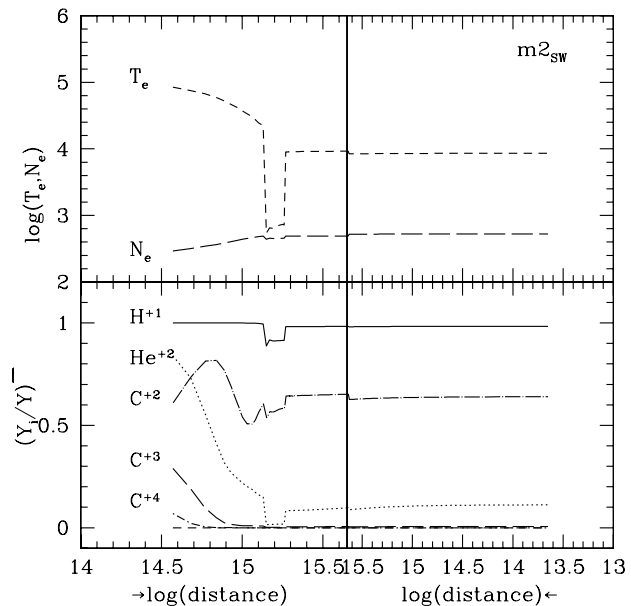


**Figure 2.** The same as for Fig. 1 for model  $m2_{SW}$ . The shock front is on the left and radiation reaches the right edge. The diagram is divided in two equal symmetric parts in order to give equal importance to the shock dominated region (left) and to the radiation dominated one (right).

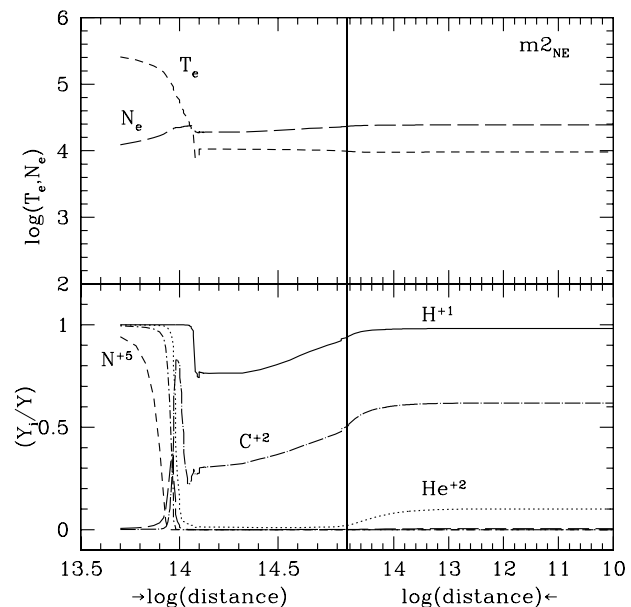


**Figure 3.** The same as for Fig. 2 for model  $m2_{NE}$ .

both black body radiation from the hot star and the (reverse) shock (see Contini & Formigini, 2000, Fig. 1). Therefore, radiation reaches the very shock front edge of the nebula. On the other hand, radiation and shock act on opposite edges of the nebula downstream of the expanding shock which propagates in the red giant atmosphere.

SUMA calculates the emitted spectrum from a gas in a plane parallel geometry. The model input parameters are

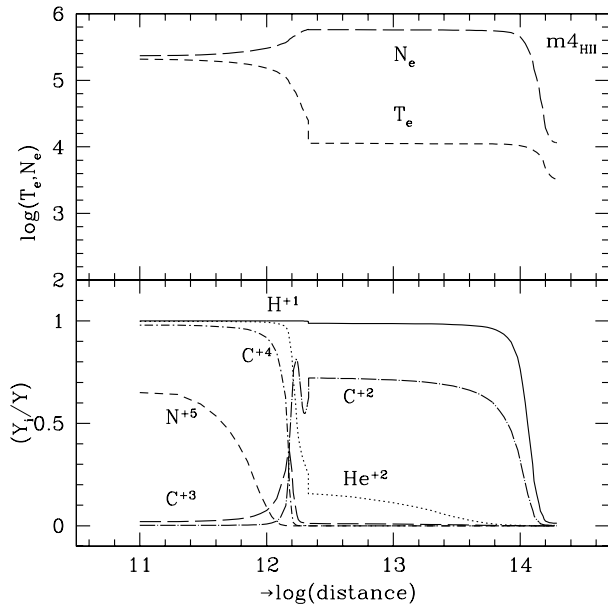


Figure 4. The same as for Fig. 1 for model  $m4_{HII}$ .

those which describe the shock (the shock velocity,  $V_s$ , the preshock density,  $n_0$ , and the preshock magnetic field,  $B_0$ ), those which represent the radiation flux (the colour temperature of the hot star,  $T_*$ , and the ionization parameter,  $U$ ), the geometrical thickness of the emitting nebulae,  $D$ , the dust-to-gas ratio,  $d/g$ , and the relative abundance to H of the elements, He, C, N, O, Ne, Mg, Si, S, A, and Fe.

The choice of the input parameter ranges is described in the following.

The radiation flux from the hot star is a black body distribution of temperature  $T_*$  selected by the best fit of the line ratios ( $NV/CIV$ ,  $HeII/H\beta$ ,  $CIII]/CIV$ , etc.).  $T_*$  was evaluated to 40 000 K by Bulgarella et al (1992) leading, however, to underpredicted HeII lines, and between 50 000 K and 60 000 K by Meier & Kafatos (1995) by the Zanstra method. They claim that the NV excitation would need a higher  $T_*$ , up to 80,000 K, and they also claim that "the overall ionization state obtained by IUE does not provide evidence for such high state of ionization". However, the ionization structure of the emitting nebulae is not easily predicted. We will select  $T_*$  by the best fit of the line ratios (Sect. 3.1.1).

We adopt  $B_0$  between  $10^{-3}$  -  $10^{-4}$  gauss, that was found for other symbiotic systems. The relatively high magnetic field is in agreement with the magnetic field in the environments of isolated giants (Bohigas et al. 1989).

$V_s$  is indicated by the FWHM of the line profiles, although the shock velocity is not exactly the velocity of the gas. Hollis et al (1991, Fig. 3) suggest velocities of  $\sim 150$   $\text{km s}^{-1}$  in the jets and of  $\sim 90$   $\text{km s}^{-1}$  in the HII region. However, Michalitsianos, Perez, & Kafatos (1994) give evidence to velocities up to 300  $\text{km s}^{-1}$  (see Sect. 5).

$n_0$  is selected from the ratio of typical lines. Notice, however, that the lines are emitted from the gas downstream, where compression leads to a density  $> n_0$  by a factor which depends on  $V_s$ ,  $B_0$ , and  $n_0$ .

The geometrical thickness of the emitting nebula,  $D$ , is

determined phenomenologically by the best fitting models but is constrained by the dimensions of the system.

We adopt relative abundances close to solar ( $He/H=0.1$ ,  $C/H=3.3 \cdot 10^{-4}$ ,  $N/H=10^{-4}$ ,  $O/H=5 \cdot 10^{-4}$ ,  $Ne/H=8.3 \cdot 10^{-5}$ ,  $Mg/H=2 \cdot 10^{-5}$ ,  $Si/H=3.3 \cdot 10^{-5}$ ,  $S/H=1.6 \cdot 10^{-5}$ ,  $Ar/H=6.3 \cdot 10^{-6}$ , and  $Fe/H=4 \cdot 10^{-5}$ ) as a first guess, refining them by the fitting process of the spectra emitted from different regions throughout the system.

A dust-to-gas ratio by mass,  $d/g = 4 \cdot 10^{-4}$  is used for all models.

To obtain the best fit of calculated to observed data the spectra emitted from the different nebulae within the R Aquarii system are summed up adopting relative weights. The relative weight,  $w$ , is proportional to the emitting area of the nebula corresponding to a model.

The models are described in Table 1.

For sake of clarity in the following, models referring to single nebulae are indicated with  $m$  (e.g.  $m1_{SW}$ ); models referring to averaged results are indicated by the capital  $M$  (e.g.  $M1_{NE}$ ).

### 3 LINE SPECTRA FROM THE JETS

In the present investigation we will treat the optical and UV spectra separately, because of the different sizes of the entrance apertures (see Hollis et al. 1992). The observations in the optical range by Hollis et al (1991) have been obtained in November-December 1989. In the UV we refer to Meier & Kafatos (1995) who analysed a set of good signal-to-noise low resolution IUE spectra of R Aqr, between 1979 and 1992. The compact HII region and the NE jet were observed in several epochs, while for the SW jet only two spectra are available. The line intensity errors were evaluated to 4 % - 5% for the strongest lines and up to 10 % - 15 % for the moderately exposed ones.

The input parameters suggested by Hollis et al. (1991) are taken as a first choice; they are, however, modified in order to achieve the best agreement with the data.

#### 3.1 The SW jet

First we consider the SW jet, which corresponds to the A' feature in Meier & Kafatos (1995, Fig. 1, bottom). The aperture of the spectrograph was carefully positioned to receive only the jet contribution, and the data by Meier & Kafatos (1995, Table 2C) represent the emission solely from the SW jet (S. R. Meier, private communication).

##### 3.1.1 The optical line ratios

In Table 2 the optical observed line intensity ratios to  $H\beta$  (column 2) are compared with model results (columns 3, 4, and 5). Although the high  $[OII]/H\beta$  and  $[OIII] 5007+/H\beta$  line ratios suggest that a shock dominated (SD) model should explain the optical spectrum, the  $[SII] 6717/6730$  line ratio ( $> 1$ ) is not well fitted by model  $m1_{SW}$ , which is characterized by  $U=0$  and a high  $n_0$ .

So, another component must be considered with lower  $n_0$  (and  $V_s$ ). We present in Table 1 the radiation dominated (RD) model  $m2_{SW}$  calculated with  $n_0 = 100 \text{ cm}^{-3}$ ,  $V_s = 80 \text{ km s}^{-1}$  and  $T_* = 80 \text{ 000 K}$ . The weighted sum of the two

Table 1  
The models adopted in Table 2, Table 3, and Table 4

	m1 <sub>SW</sub>	m2 <sub>SW</sub>	m1 <sub>NE</sub>	m2 <sub>NE</sub>	m3 <sub>NE</sub>	m4 <sub>NE</sub>
H $\beta$ (erg cm <sup>-2</sup> s <sup>-1</sup> )	3.7(-3)	3.2(-4)	0.122	0.078	0.08	4.(-4)
V <sub>s</sub> (km s <sup>-1</sup> )	150.	80.	120.	140.	150.	50.
n <sub>0</sub> (cm <sup>-3</sup> )	4(3)	100.	7.(3)	4.(3)	4.(3)	50.
B <sub>0</sub> (gauss)	1(-3)	1.(-4)	1.(-3)	1.(-3)	1.(-3)	1.(-4)
D (10 <sup>15</sup> cm)	2.5	9.	1.4	1.4	1.4	10.
U	-	2.3(-3)	1.6(-3)	2.2(-3)	2.2(-3)	1.(-3)

Table 2  
Optical line intensities relative to H $\beta$ =1 in the jets

line	obs(SW) <sup>1</sup>	m1 <sub>SW</sub>	m2 <sub>SW</sub>	M <sub>SW</sub> (opt) <sup>2</sup>	obs(NE) <sup>1</sup>	m2 <sub>NE</sub>	m3 <sub>NE</sub>
[OII] 3727+	10.11	10.7	5.0	9.53	2.3	2.66	3.0
[NeIII] 3869+	2.68	2.6	1.0	2.4	0.85	1.1	1.3
[SII] 4069+	0.33	1.1	0.04	0.70	0.44	0.7	1.
[OIII] 4363	0.67	1.3	0.27	1.0	0.14	0.10	0.1
HeI 4471	< 0.28	0.17	0.06	0.15	0.08	0.05	0.06
[OIII] 5007+	15.14	15.6	8.2	14.1	4.2	4.05	4.2
[NI] 5200+	< 0.28	0.18	0.01	0.15	0.09	1.(-5)	1.(-5)
[NII] 5755	0.74	0.4	0.04	0.33	0.09	0.09	0.1
HeI 5876	0.80	0.53	0.20	0.5	0.12	0.15	0.16
[OI] 6300+	< 0.8	0.9	0.05	0.72	0.62	0.23	0.4
[NII] 6548+	5.45	6.	2.19	5.2	3.17	4.6	5.0
[SII] 6717	0.73	0.8	0.27	0.7	0.25	0.22	0.3
[SII] 6730	0.63	1.3	0.26	1.0	0.41	0.49	0.7
[OII] 7322+	< 0.28	6.7	0.23	5.3	0.87	0.8	1.1
[SIII] 9069+	< 0.56	1.17	2.66	1.47	1.34	2.4	1.6
CIV 1550	-	91.7	5.56	-	-	-	-
w <sup>3</sup>	-	1.	3.	-	-	-	-

<sup>1</sup> Hollis et al. (1991, Table 3)

<sup>2</sup> The averaged line ratio is :

$$I_{\lambda}/I_{H\beta} = ((I_{\lambda}/I_{H\beta})_1 H\beta_1 w_1 + (I_{\lambda}/I_{H\beta})_2 H\beta_2 w_2) / (H\beta_1 w_1 + H\beta_2 w_2)$$

<sup>3</sup> relative weight

models, M<sub>SW</sub>(opt), is given in Table 2, column 5. Model m2<sub>SW</sub> shows some discrepancies for most of the line ratios, but a better fit to [SII] 6717/6730, and most importantly, it leads to a better agreement of the summed spectrum with the data (Table 2). An RD model, corresponding to n<sub>0</sub>=65 cm<sup>-3</sup>, which provides [OIII]/H $\beta$  and [OII]/H $\beta$  better fitting the observations was discarded when modelling the UV spectra ((Sect. 3.1.2). In fact, optical and UV spectra are modelled consistently, and the RD model is chosen cross-checking the results in the UV ranges, until a fine tuning is obtained. Adopting w(m1<sub>SW</sub>) : w(m2<sub>SW</sub>) :: 1: 3 (last row of Table 2), which leads to the best fit of the observed optical spectrum, the [SII] line ratio is still lower than observed in the averaged spectrum. In fact, H $\beta$  corresponding to m2<sub>SW</sub> is by a factor of  $\sim 10$  lower than H $\beta$  calculated by m1<sub>SW</sub>.

The colour temperature of the hot star T<sub>\*</sub>=80 000 K, which is adopted to explain the optical spectrum from the SW jet, was selected from a large grid of models calculated with different T<sub>\*</sub>. This temperature was found too high by Meier & Kafatos to match all the UV spectral line fluxes. However, compression downstream of the shock front leads

to high densities which speed up the cooling rate and a region of low temperature gas also appears inside the nebula.

For sake of consistency, this value will be adopted hereafter to model the spectra from the NE jet and the HII region.

### 3.1.2 The evolution of the UV spectra

Model results for the SW jet are given in Table 3 and are compared with the data in Table 4.

The line ratios are given relative to CIV, which is generally a strong line. However, high CIII]/CIV and CII]/CIV (> 1) characterize the R Aqr UV line spectra. The spectra which appear in columns 3 and 5 of Table 4 (M1<sub>SW</sub> and M2<sub>SW</sub>, respectively) represent the weighted sums of the two models, m1<sub>SW</sub> and m2<sub>SW</sub>, that were selected by fitting the optical lines (Table 1). The summed spectra in the two epochs correspond to different relative weights of the SD and RD models. Adopting, on the other hand, the relative weights indicated by the best fit of the optical lines we could not obtain an acceptable agreement to the observed UV line ratios. Different relative weights (w(SD) : w(RD)) :: 1 : 300 in

Table 3  
UV line models ( $H\beta=1$ )

line	m1 <sub>SW</sub>	m2 <sub>SW</sub>	m1 <sub>NE</sub>	m2 <sub>NE</sub>	m3 <sub>NE</sub>	m4 <sub>NE</sub>
NV 1238+42	38.9	1.9(-3)	1.2	1.5	1.67	5.(-6)
CII 1334+36	20.	2.6	0.93	0.8	0.87	1.1
SiIV + OIV] 1394+	69.0	2.2	2.6	2.97	2.9	0.22
NIV] 1483+86	22.0	0.4	1.1	0.9	1.0	7.2(-3)
CIV 1548+51	92.0	5.56	3.9	3.87	4.	0.068
HeII 1640	0.6	0.33	0.23	0.3	0.29	0.4
OIII] 1661+66	10.2	1.62	0.45	0.54	0.55	0.45
NIII] 1749+54	11.0	1.6	0.40	0.5	0.5	0.44
SiII 1808+17	0.5	0.06	0.083	0.075	0.12	0.05
SiIII] 1883+92	16.3	2.4	0.72	0.69	0.76	1.5
CIII] 1907+10	46.	9.46	2.3	2.6	2.85	2.2
[OIII] + CII] 2321+	21.2	2.5	2.1	1.54	2.1	1.8
[OII] 2470	5.8	0.3	0.78	0.67	0.9	0.15
MgII 2795+	0.23	0.06	0.38	0.32	0.45	0.73
HeII 3203	0.037	0.02	0.014	0.018	0.018	0.024
w	1	300	1	1	1	350

<sup>1</sup> relative weight

Table 4  
UV line intensities relative to CIV (SW Jet)

line	28/12/1989	M1 <sub>SW</sub>	27/5/1991	M2 <sub>SW</sub>
NV 1238+42	0.19	0.17	0.17	0.15
CII 1334+36	0.47	0.45	0.5	0.42
SiIV 1394	0.31	0.56	0.3	0.54
OIV] 1401+07	0.062	↑	0.3	↑
NIV] 1483+86	0.16?	0.14	0.16?	0.13
CIV 1548+51	1.	1.	1.	1.
HeII 1640	0.1	0.077	0.08	0.08
OIII] 1661+66	0.33	0.22	0.31	0.24
NIII] 1749+54	0.30	0.22	0.39	0.23
SiII 1808+17	0.06	0.008	-	0.008
SiIII] 1883+92	0.27	0.31	0.48	0.32
CIII] 1907+10	> 1.28	1.20	> 1.47	1.24
w(SD): w(RD)	-	1:300	-	1:350

1989 and w(SD) : w(RD) :: 1: 350 in 1991, instead of 1 : 3 as in the optical range) lead to the best fit of the UV spectra. Although the fit is rough the trend is rather save. Considering the observational errors, such a small difference in the relative weights could be in agreement with non-variability of the spectra.

In order to better understand the results, the distribution of the fractional abundance of some significant ions, as well as the distribution of the temperature and density throughout the SD and RD nebulae are given in Fig. 1 and Fig. 2, respectively.

The high relative weight of the RD model indicates that a large region of gas, affected by photoionization from the hot star and corresponding to characteristics closer to the ISM, contributes to the observed fluxes. The extended region shows, in fact, relative small densities and velocities not exactly fitting the conditions of the jet bulk.

The increasing weight of the RD model with time could explain the decline of the SW jet. In fact, more IS matter is

swept up by the shock at latest epochs. A larger contribution corresponds to weaker fluxes because the RD model is characterized by relatively low densities and velocities. To obtain the distance  $r$  of the SW jet from the hot source, recall that the fluxes are calculated at the nebula. Adopting a distance  $d = 200$  pc, the data from Meier & Kafatos (1995, Table 2C), and the results of model m1<sub>SW</sub>, we compare the observed and calculated fluxes of the NV line,  $1.5 \cdot 10^{-13} \times (200 \text{ pc})^2 = 38.9 \times 0.0037 \times r^2$ . The distance of the bulk of the SW jet from the center of the system results  $r \sim 6 \cdot 10^{14}$  cm.

### 3.2 The NE jet

The NE jet is outlined in Meier & Kafatos (1995, Fig. 1) and encompasses the regions A, B, and D in VLA 6 cm observations.

### 3.2.1 The optical line ratios

The observed optical lines are from Hollis et al. (1991, Table 3) and sample the regions near the peak of the jet emission.

The optical spectrum (Table 2) is explained by a composite model (m2<sub>NE</sub>) characterized by a shock of 140 km s<sup>-1</sup>, T<sub>\*</sub>=80 000 K, and a rather low U=2.2 10<sup>-3</sup>. Some line ratios (HeI/Hβ, [OIII]/Hβ, [OI]/Hβ, and [SIII]/Hβ) are better fitted by a similar model with V<sub>s</sub>=150 km s<sup>-1</sup> (m3<sub>NE</sub>).

A low U, reduced by dilution, confirms that the NE jet is rather far away from the hot star. The distance r of the emitting nebula in the jet from the hot star is calculated relating the photon flux from the hot star,  $\mathcal{N}$  with the ionization parameter:  $\mathcal{N} (R_{hot}/r)^2 = U n c$ , where n is the density and R<sub>hot</sub> = 5 10<sup>8</sup> cm is the radius of the hot star. Adopting n = 3 10<sup>4</sup> cm<sup>-3</sup> from Fig. 3, r results 2 10<sup>15</sup> cm.

### 3.2.2 The evolution of the UV spectra

Table 3 shows the UV spectra calculated by models m1<sub>NE</sub>, m2<sub>NE</sub>, m3<sub>NE</sub>, and m4<sub>NE</sub> which are selected to fit the spectra of the NE jet in different epochs. Model m4<sub>NE</sub>, which is characterized by conditions closer to those of the ISM, is similar to m2<sub>SW</sub> (Table 1, column 3) that was found to improve the fit of the SW jet spectrum (relatively low V<sub>s</sub>, n<sub>0</sub>, B<sub>0</sub>, and a large D). The models are all RD dominated. The line ratios refer to Hβ=1. In order to understand the line ratios, we present in Fig. 3 the distribution of the fractional abundances of the most significant ions, as well as of the temperature and density throughout the nebula corresponding to model m2<sub>NE</sub>.

In Table 5 we compare model results with spectra at different epochs for the NE jet. The data (Meier & Kafatos 1995, Table 2B) represent the fluxes at different epochs. We could not use line ratios to CIV, as in Table 4, because the CIV line is saturated. Viotti et al. (1987) in 1985 Dec 23-25 measured the CIV flux of 28.8 10<sup>-13</sup> erg cm<sup>-2</sup> s<sup>-1</sup>. This value is intermediate between the 1983 flux and the 1986 lower limit (Table 5).

We obtain an acceptable fit of the data summing up m2<sub>NE</sub> with model m4<sub>NE</sub> (Table 1, last column). The spectra resulting from the weighted sum of m1<sub>NE</sub>, m2<sub>NE</sub>, and m3<sub>NE</sub> with model m4<sub>NE</sub> are presented in Table 5 (M1<sub>NE</sub>, M2<sub>NE</sub>, and M3<sub>NE</sub>, respectively). The relative weights appear in the last row of Table 3. The arrows indicate that SiIV and OIV] line fluxes are summed up.

The fit is acceptable, although Table 5 shows that SiII, [OII], and MgII are lower than observed. The calculated fluxes of the SiIV and SiIII] lines are higher than observed and could indicate that Si is partly locked into dust grains. The anomalous flux of the HeII 3203 line can be due to the fact that it falls at the IUE sensitivity limit.

The errors in observations and in model calculations do not permit to distinguish between the physical conditions in the emitting gas between December 1987 and June 1989.

As found for the optical lines, a model with V<sub>s</sub>=150 km s<sup>-1</sup> (m3<sub>NE</sub>) explains the spectra at later epochs. Therefore, in Table 5 this model is compared with both the spectra at 1987 and 1989, while the model with V<sub>s</sub>=140 km s<sup>-1</sup> better fits the conditions at 29/12/1986.

A sensible difference of line fluxes is noticed between May 1983 and December 1986. Although many different

models should be considered, we have adopted model m4<sub>NE</sub> with the same weight as in 1986-1989 and model m1<sub>NE</sub> characterized by a lower velocity and a higher density than m3<sub>NE</sub>. This suggests that the shock has accelerated with time propagating outwards the system, throughout the decreasing density gradient of the red giant atmosphere (Contini 1997).

The ionization parameter U increasing at later epochs indicates that it changes with the Mira pulsation period, rather than with dilution. The jets are perpendicular to the accretion disk and to the orbital plane. Therefore, obscuration of the hot source is due to dusty material ejected by the Mira. A time interval of 3.6 years between May 1983 and December 1986 corresponds to 3.4 pulsation periods, leading to a different U.

We can now calculate the distance r of the NE jet from the binary system in the different epochs. Comparing the observed NV 1240 flux at Earth in 1987 (15.2 10<sup>-13</sup> erg cm<sup>-2</sup> s<sup>-1</sup>) with the flux calculated by model m3<sub>NE</sub>, r results 2 10<sup>15</sup> cm and in 1986 r = 1.8 10<sup>15</sup> cm. In 1983 the flux of NV was 8.6 10<sup>-13</sup> erg cm<sup>-2</sup> s<sup>-1</sup> and r=1.4 10<sup>15</sup> cm, indicating that the NE jet has slightly farthened from the central system between 1983 and 1987.

To calculate the distance of the low density region we consider the HeII 1640 line in m4<sub>NE</sub> and find r= 2.26 10<sup>15</sup> cm. The results confirm that different conditions coexist in the complex region representing the jets.

In conclusion, the observed trend of increasing line fluxes with time is explained by a slight acceleration of the shock expanding in the surrounding of the binary system.

## 4 THE HII REGION

We present in Table 6 the best fitting model of the spectra emitted by the HII region in the different epochs. The data are taken from Meier & Kafatos (1995, Table 2A). The position of the IUE spectrograph aperture integrates both the features identified as part of the HII region, as well as the SW jet region (Meier & Kafatos). However, the fluxes emitted from the jets are by a factor  $\geq 3$  lower than those from the HII region, so we will refer to these data as representative of the HII region, with a minor contamination of the jets.

The models are described in the bottom of Table 6. For all epochs a preshock density of 6 10<sup>4</sup> cm<sup>-3</sup> and V<sub>s</sub> slightly higher than 100 km s<sup>-1</sup> explains almost all of the line ratios. These conditions correspond to a postshock density of  $\geq 6 \cdot 10^5$  cm<sup>-3</sup>. Notice, however, that the magnetic field also plays an important role in downstream compression. We have found B<sub>0</sub>=2 10<sup>-3</sup> gauss, which is rather high, thus preventing a large compression. A geometrical thickness, D = 2 10<sup>14</sup> cm leads to the best agreement of calculated with observed spectra.

The models adopted in Table 6 (m1<sub>HII</sub>, m2<sub>HII</sub>, m3<sub>HII</sub>, and m4<sub>HII</sub>) are calculated considering that the shock and the photoionising flux act on the same edge of the emitting nebula.

This condition corresponds to the reverse shock, which was created by collision of the winds between the stars (Sect. 2).

The distribution of the fractional abundance of some

Table 5  
UV line fluxes in the NE jet ( $10^{-13}$  erg cm $^{-2}$  s $^{-1}$ )

	25/5/1983	M1 <sub>NE</sub>	29/12/1986	M2 <sub>NE</sub>	31/12/1987	M3 <sub>NE</sub>	5/6/1989
NV 1238+42	8.6	6.0	11.5	12.0	15.2	14.0	14.9
CII 1334+36	7.9	10.4	13.8	21.6	14.7	22.7	16.5
SiIV 1394	5.4	13.4	9.1	25.7	10.1	31.8	11.7
OIV] 1401+07	8.1	↑	11.9	↑	15.4	↑	16.6
NIV] 1483+86	-	5.0	9.8	7.12	10.0	8.3	9.9
CIV 1548+51	14.6	19.4	>30.8	31.0	>39.6	33.5	>40.5
HeII 1640	4.0	3.4	8.0	7.94	10.0	8.0	9.5
OIII] 1661+66	7.2	5.0	13.2	10.5	15.0	11.0	16.5
NIII] 1749+54	6.2	5.0	10.6	10.0	11.7	10.5	13.2
SiII 1808+17	-	0.7	4.4	1.3	5.5	1.6	7.2
SiIII] 1883+92	5.5	12.	12.3	26.4	15.5	27.2	15.7
CIII] 1907+10	>15.7	23.	>27.5	51.1	>30.4	53.7	>33.8
[OIII]+CII] 2320+	13.2	20.	38.4	37.2	51.7	41.5	51.2
[OII] 2470	8.0	5.0	14.4	7.0	20.3	9.1	20.2
MgII 2795+	14.2	6.0	18.5	12.7	25.9	13.7	23.9
HeII 3203	-	0.18	-	0.5	8.1	0.4	6.6

<sup>1</sup> The observed data are in  $10^{-13}$  erg cm $^{-2}$  s $^{-1}$

Table 6  
UV line intensities relative to CIV (HII region)

	8/11/1980	m1 <sub>HII</sub>	25/5/1983	m2 <sub>HII</sub>	25/10/1986	m3 <sub>HII</sub>	26/5/1991	m4 <sub>HII</sub>
NV 1238+42	-	0.11	-	0.11	0.27	0.26	0.20	0.22
CII 1334+36	0.33	0.30	0.29	0.29	0.27	0.24	0.28	0.23
SiIV 1394	0.22	0.1	0.21	0.1	0.23	0.1	0.27	0.1
OIV] 1401+07	0.32	0.32	0.30	0.31	0.29	0.26	0.27	0.24
NIV] 1483+86	-	0.2	0.26?	0.2	0.27	0.22	0.2	0.22
CIV 1548+51	1.	1.	1.	1.	1.	1.	1.	1.
HeII 1640	0.33	0.33	0.26	0.29	0.2	0.18	0.18	0.174
OIII] 1661+66	0.55	0.33	0.45	0.29	0.35	0.2	0.32	0.2
NIII] 1749+54	0.5	0.4	0.42	0.33	0.35	0.22	0.28	0.2
SiII 1808+17	0.28	0.11	0.18	0.12	0.09	0.08	0.14	0.08
SiIII] 1883+92	>0.63	1.1	0.79	0.88	0.54	0.5	0.38	0.45
CIII] 1907+10	>1.2	2.9	>1.66	2.6	>1.18	1.48	>0.95	1.4
[OIII]+CII] 2320+	>1.2	1.3	1.26	1.34	0.67	1.12	0.9	1.08
[OII] 2470	0.7	0.8	0.74	0.87	0.4	0.66	0.43	0.64
MgII 2795+	>1.17	0.3	1.8	0.32	0.67	0.25	0.6	0.24
HeII 3203	-	0.02	-	0.017	0.39	0.011	0.27	0.01
H $\beta$ (erg cm $^{-2}$ s $^{-1}$ )	-	4.86	-	4.5	-	3.29	-	3.02
CIV/H $\beta$	-	1.	-	1.	-	1.56	-	1.6
V <sub>s</sub> (km s $^{-1}$ )	-	110	-	110	-	125	-	120
n <sub>0</sub> (cm $^{-3}$ )	-	6(4)	-	6(4)	-	6(4)	-	6(4)
B <sub>0</sub> (gauss)	-	2(-3)	-	2(-3)	-	2(-3)	-	2(-3)
D (10 $^{14}$ )	-	2.	-	2.	-	2.	-	2.
T <sub>*</sub> (K)	-	8(4)	-	8(4)	-	8(4)	-	8(4)
U	-	1(-2)	-	8.5(-3)	-	6(-3)	-	5.5(-3)

significant ions, as well as of the temperature and density downstream of the reverse shock are given in Fig. 4,

Table 6 shows that NV/CIV slightly changes with time, while HeII/CIV decreases. The results of model calculations generally show that NV/CIV increases with V<sub>s</sub>, while HeII/CIV and CIII]/CIV increase with both T<sub>\*</sub> and U. The ionization parameter is diluted by distance, suggesting, therefore, that the shock front is slightly farthening from the hot source. The distance from the hot source in 1991,

calculated by comparing the HeII line is 8.8 10<sup>13</sup> cm, while in 1980 the distance is 8.6 10<sup>13</sup> cm. The difference is negligible, considering the errors in the data and in the models. Therefore, the reverse shock is most probably a standing shock.

The agreement of model results with the data is good enough and indicates that the contribution of the expanding shock is negligible. In fact, the expanding shock, many years after collision, has reached the outskirts of the sys-

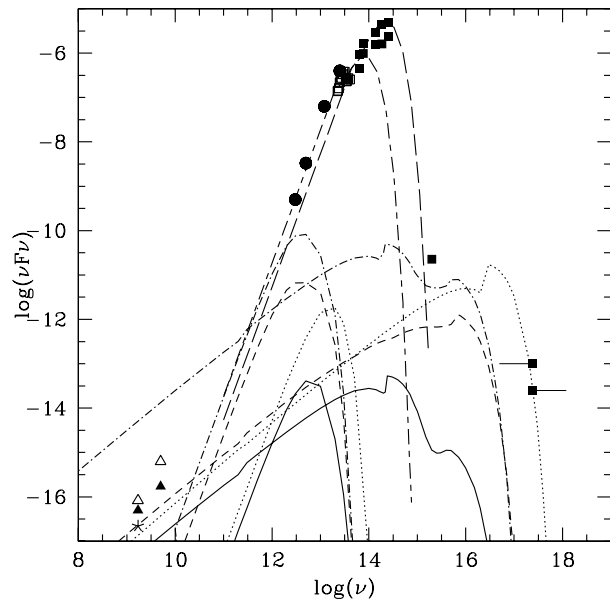


**Figure 5.** The comparison of the observed continuum SED with model results (see text). Solid lines represent the HII region ( $m_{4HII}$ ); short-dashed lines refer to the SW jet ( $m_{1SW}$ ), dash-dotted lines to the NE jet ( $m_{2NE}$ ), and dotted lines to the model calculated with  $V_s=300 \text{ km s}^{-1}$ .

tem. Here, the density is relatively low ( $10^3 \text{ cm}^{-3}$ ) and the nebula downstream of the expanding shock is reached by a weak radiation flux. Therefore, the intensity of the lines is by at least a factor of  $10^4$  lower than the intensity of the lines emitted downstream of the reverse shock.

## 5 THE SED OF THE CONTINUUM

In Fig. 5 we compare the observed continuum SED with the calculated SEDs of the models corresponding to the prevailing conditions in the R Aqr system.

The data in the near-IR (filled squares) come from Le Bertre (1993), those in the mid-IR (open squares) from Monnier, Geballe, & Danchi (1998), in the far-IR are taken from IRAS (filled circles). The data in the radio range come from Dougherty et al (1995). The fluxes from the different features corresponding to the central region (open triangles) and to the jets (filled triangles) have been summed up.

A black-body radiation with a temperature of  $T=2800 \text{ K}$  (long-dashed line) represents the red giant (Anandarao & Pottasch 1986, Meier & Kafatos 1995). Moreover, we have added a black-body emission corresponding to  $T=1000 \text{ K}$  (long-dash-short-dash line) to represent emission from dust in the inner radius of the Mira (see Tuthill et al 2000). Absorption by silicates at  $\sim 9.7 \mu\text{m}$  is clearly noticed.

The models were selected by modelling the line spectra in previous sections. Each model corresponds to two curves, one is bremsstrahlung radiation from the gas and the other is reradiation by dust in the IR. Dust grains and gas are coupled entering the shock front and mutually heat each other (Viegas & Contini 1994). So, high velocity models correspond to mid-IR emission and low velocity models

to far-IR. In the present case, there are no data in the very far-IR to constrain the dust-to-gas ratio ( $d/g = 4 \cdot 10^{-4}$  is used in the models) in the jet regions. However, Fig. 5 shows that most of the corresponding frequency range is occulted by the black-body emission from the red giant.

The models are represented in Fig. 5 according to the relative weights. They are constrained only by the datum in the UV (from Kafatos, Michalitsianos, & Hollis 1986) and by the data in the radio. Model results should be summed up to best fit the UV datum, however, they are shown one by one in order to better understand single model contributions in the different frequency ranges. Solid lines refer to model  $M_{4HII}$  which represents the HII region and corresponds to a shock velocity of  $V_s=120 \text{ km s}^{-1}$ . Short-dashed lines correspond to the SD model  $m_{1SW}$ , dash-dotted lines correspond to model  $m_{2NE}$ .

Dotted lines in Fig. 5 refer to the model calculated with  $V_s=300 \text{ km s}^{-1}$  and  $n_0=1000 \text{ cm}^{-3}$  (Michalitsianos et al. 1994). Relatively high velocities can survive when high velocity gas in the jets collides with ISM inhomogeneities with a relatively low density. A shock velocity of  $300 \text{ km s}^{-1}$  corresponds to a temperature of  $1.4 \cdot 10^6 \text{ K}$  in the post shock region. This temperature is responsible for soft X-ray emission observed by Chandra below  $1.5 \text{ KeV}$ , while the hard X-ray emission observed from the central region of the system comes from the accretion disk (Kellogg, Pedelty, and Lyon 2001).

The optical and UV spectra, however, calculated with  $V_s=300 \text{ km s}^{-1}$  and  $n_0 < 1000 \text{ cm}^{-3}$

are weak compared with the spectra calculated for the jets and the HII region (see Sects. 3 and 4) because a) the gas at a temperature of  $\sim 10^6 \text{ K}$  will hardly recombine at a distance within the dimension of the system and b) line intensities are  $\propto n^2$ . The  $H\beta$  flux calculated with  $n_0 = 1000 \text{ cm}^{-3}$  would be  $\sim 4.3 \cdot 10^{-7} \text{ erg cm}^{-2} \text{ s}^{-1}$  (cf. Table 1). The corresponding NV and CIV lines are weak but observable and may appear in the wings of the line profiles as the contribution of a relatively broad component. So, this model explains the soft X-ray data in the SED of the continuum, but its contribution to the line spectra is negligible. This problem, however, awaits new higher resolution/higher sensitivity space UV observations.

Fig. 5 shows that the radio data in the different positions follow a thermal curve in agreement with Dougherty et al (1995). Bremsstrahlung radiation from the NE jet overpredicts the data in the radio. Recall that self-absorption increases with wavelength and can reduce emission at  $\nu < 10 \text{ GHz}$  (Contini 1997).

## 6 CONCLUDING REMARKS

In the previous sections we have analysed the optical spectra emitted from the jets and the temporal evolution of the UV spectra from the jets and from the HII region. We have demonstrated throughout the modelling of the different regions of R Aqr that the coupled effect of radiation from the hot star and shocks give a consistent explanation to some of the questions raised by the observational evidence.

The modelling of the spectra indicates a temperature of  $T_* = 80 \text{ 000 K}$  for the hot white dwarf component of the R Aqr system. This high temperature, already suggested by



Meier & Kafatos, is justified by the consistent account for the shocks.

The time evolution of the NE jet is thus explained by the decreasing of the density gradient in the outer region of the system and by a small change in the obscuration of the hot source by the Mira dusty envelope. The spectral evolution of the NE jet indicate that between 29/12/1986 and 5/6/1989 the shock velocity has increased by a very small factor, from  $140 \text{ km s}^{-1}$  to  $150 \text{ km s}^{-1}$ . At earlier epochs (25/5/1983) the physical conditions of the emitting gas were slightly different, corresponding to lower  $V_s$  ( $120 \text{ km s}^{-1}$ ), a higher density by a factor of  $\sim 1.8$ , and a lower  $U$  by a factor of  $\sim 1.4$ .

The decrease of the SW UV line intensities between 1989 and 1991 is due to the increased contribution of low density-velocity interstellar matter from the region of the jet at later epochs.

In the HII region the evolution of the UV spectra from 8/11/1980 to 26/5/1991 indicates that the reverse shock is quite likely a standing shock.

The results obtained by modelling the line spectra are cross-checked by the fit of the continuum SED. It is found that a black-body temperature of 2800 K reproduces the radiation from the red giant and an additional component of black-body emission of 1000 K is emitted by dust from the envelop of the red giant.

Model calculations confirm that the radio emission is of thermal origin, however, the contribution of synchrotron radiation, created by Fermi mechanism at the shock front, cannot be excluded.

We found that the bulk region of the NE jet emission is at a distance of about  $2 \cdot 10^{15}$  cm from the binary system in 1987, and for the SW jet is at  $\sim 6 \cdot 10^{14}$  cm. The distance of the reverse shock from the hot source is about  $9 \cdot 10^{13}$  cm.

The magnetic field varies from  $2 \cdot 10^{-3}$  gauss in the HII region to a minimum of  $10^{-4}$  gauss in the extended region. In the bulk of the jets we found  $B_0 = 10^{-3}$  gauss. Recall that turbulence created by Rayleigh-Taylor instabilities near the shock front may increase the magnetic field by some orders (see Contini & Prialnik 1997).

## 7 ACKNOWLEDGMENTS

We are very grateful to the referee for many interesting remarks that highly improved the presentation of the paper.

## REFERENCES

Anandarao B.G., Pottasch S.R. 1986, *A&A*, 162, 167.  
 Baade, W. 1943 *Ann. Report Dir. Mt. Wilson Obs.*, No 1942-1943, 17.  
 Binette L., Dopita M. A., Tuohy I.R. 1985, *ApJ*, 297, 476.  
 Burgarella D., Vogel M., Paresce F. 1992, *A&A*, 262, 83.  
 Contini M. 1997, *ApJ*, 483, 886.  
 Contini M., Prialnik D. 1997, *ApJ*, 475, 803.  
 Contini M., Formigini L. 1999, *ApJ*, 517, 925.  
 Contini M., Formigini, L. 2000, in "Thermal and Ionization aspects of the flows from hot stars : observations and theory". Lamers and Sapar eds. ASP Conference Series, Vol. 204, p. 345  
 Contini M., Formigini L. 2001, *A&A*, 375, 579.

Dougherty S.M., Bode M.F., Lloyd H.M., Davis R.J., Eyers S.P. 1995, *MNRAS*, 272, 843.  
 Formigini L., Contini M., Leibowitz E. 1995, *MNRAS*, 277, 1071.  
 Hinkle K.H., Wilson T.D., Scharlach W.W.G., Fekel F.C. 1989, *AJ*, 98, 1820.  
 Hollis J.M., Oliverson R.J., Kafatos M., Michalitsianos A.G., Wagner R.M. 1991, *ApJ* 377, 227.  
 Hollis J.M., Pedelty J.A., Lyon R.G. 1997, *ApJ*, 482, L85.  
 Kafatos M., Michalitsianos A.G., Feibelman W.A. 1982, *ApJ*, 257, 204.  
 Kafatos M., Michalitsianos A.G., Hollis J.M. 1986, *ApJS*, 62, 1853.  
 Kafatos M., Hollis J.M., Yusef-Zadeh F., Michalitsianos A.G., Elitzur M. 1989, *ApJ*, 346, 991.  
 Kellogg E., Pedelty J.A., Lyon R.G. 2001 *ApJ* 563 L151  
 Le Bertre T. 1993, *A&AS*, 97, 729.  
 Meier S.R. and Kafatos M., 1995, *ApJ* 451, 359.  
 Michalitsianos A.G., Perez M., Kafatos M., 1994, *ApJ*, 423, 441.  
 Monnier J.D., Geballe T.R., Danchi W.C 1998, *ApJ*, 502, 833.  
 Nussbaumer H. 2000 in "Thermal and Ionization aspects of the flows from hot stars : observations and theory". Lamers and Sapar eds. ASP Conference Series, Vol. 204, p. 317  
 Paresce F. et al 1991, *ApJ*, 369, L67.  
 Paresce F. and Hack W. 1994, *A&A*, 287, 154.  
 Solf, J. & Ulrich, H. 1985 *A&A*, 148, 274.  
 Tuthill P.G., Danchi W.C., Hale D.S., Monnier J.D., Townes C.H. 2000, *ApJ*, 534, 907.  
 Viegas S.M., Contini M. 1994, *ApJ*, 428, 113.  
 Viotti, R., Piro, L., Friedjung, M., Cassatella, A. 1987, *ApJ*, 319, L7.  
 Viotti, R., Badiali, M., Cardini, D., Emanuele, A., Iijima, T. 1997, in *Proc. ESA Symposium Hipparcos Venice '97*.  
 Wilson L.A., Garnavich P., Mattei J.A. 1981, *Inf. Bull. Var. Stars*, N0. 1961.